











Cite this: *Chem. Commun.*, 2024, 60, 5522

Received 19th February 2024,
Accepted 26th April 2024

DOI: 10.1039/d4cc00812j

rsc.li/chemcomm

Triptycene-based diiron(II) mesocates: spin-crossover in solution†

Riccardo Mobili, ^{*ab} Giovanni Preda, ^a Daniele Dondi, ^a Enrico Monzani, ^a
Dhanalakshmi Vadivel, ^a Chiara Massera, ^c Dario Pasini ^a and
Valeria Amendola ^{*a}

Triptycene-based diiron(II) and dizinc(II) mesocates were obtained using a novel rigid ligand with two pyridylbenzimidazole chelating units fused into the triptycene scaffold. Studies on the diiron(II) assembly in solution showed that the complex undergoes thermal-induced one-step spin-crossover with $T_{1/2}$ at 243 K (Evans method).

Triptycenes (Tp) possess a propeller-like rigid structure, with three benzene rings (the propeller blades) connected by two bridgehead sp^3 carbon atoms, defining dihedral angles of 120° .¹ This class of compounds has been garnering increasing interest among supramolecular chemists and material scientists^{1–3} for their applications in solution, including molecular machines,³ catalysis,⁴ host–guest chemistry,^{5,6} homochiral self-sorting and enantioseparation,⁷ and optoelectronics.⁸ Despite these wide applications, only very few examples of supramolecular assemblies containing Tp are known. These types of systems, such as coordination cages and helicates,^{5,6,8–11} have typically been developed using ligands with two or three binding units (e.g., pyridines) linked to a central Tp core, with metal centres such as Pd(II),⁵ lanthanides⁹ or Cu(I).¹¹ Triple-stranded dinuclear complexes (M_2L_3) are considered as the simplest examples of octahedral multinuclear assemblies.¹² When non-chiral ligands are used, racemic mixtures of the homochiral helicates (Δ, Δ and Λ, Λ) are generally obtained,^{12,13} while the diastereomeric heterochiral (Δ, Λ) mesocates¹⁴ are more uncommon. On the other hand, in an example from our group,^{13c} by mixing the racemic

mixture of chiral ditopic ligands with Cu(I), either homochiral helicates or a heterochiral mesocate could be isolated, depending on the solvent employed. Circular helicates and non-helical species are among the rare examples of Tp-based supramolecular assemblies, obtained using a flexible ditopic chelating ($N^{\wedge}O$) ligand and Zn(II).^{6a} More recently, triple-stranded M_2L_3 helicates have been developed using Ga(III) ions and Tp-based bis-catecholate ligands.^{6b} The corresponding negatively-charged assemblies have been employed as molecular hosts for tetraalkylammonium cations. Among triple-stranded polynuclear complexes, Fe(II) assemblies have raised particular interest over the last two decades as spin-crossover materials.¹⁵ Spin-crossover (SCO) is a noteworthy phenomenon, wherein the application of an external stimulus (e.g. temperature, pressure, light irradiation, guest inclusion) induces the reversible switch between high-spin (HS) and low-spin (LS) states.^{15–23} This reversible spin-state conversion is generally accompanied by a change in the physico-chemical properties of the complex (e.g. UV-vis. absorption, mechanical properties, electrical resistance, magnetic moment), thus leading to potential applications of SCO complexes in electronics, spintronics, sensing and information processing.¹⁶ To the best of our knowledge, there are currently no examples of spin-crossover systems containing Tp and Fe(II).

In this work, the rigid ligand **L** (Fig. 1), consisting of a triptycene core and two pyridylbenzimidazole moieties, was used to synthesize M_2L_3 complexes with Fe(II) and Zn(II). Additionally, the thermal-induced spin-crossover (SCO) behaviour of the diiron(II) complex was investigated in solution by means of ¹H-NMR and UV-vis spectroscopy.

The ligand **L** was synthesized following a procedure recently described by our group^{2b} (see the ESI† for details). The final product was obtained as a brownish solid in moderate yield. The ¹H-NMR characterization showed that **L** exists in solution as an equimolar mixture of two tautomers, which differ on the basis of the relative position of the benzimidazole N-Hs with respect to the Tp core: same side (*syn*) and opposite side (*anti*), see Fig. S1b (ESI†).^{2b}

The Fe(II) and Zn(II) complexes were prepared by adding the corresponding triflate salt to a suspension of the ligand in

^a Department of Chemistry, University of Pavia, viale Torquato Taramelli 12, 27100 Pavia, Italy. E-mail: valeria.amendola@unipv

^b Sorbonne Université, CNRS, Institut Parisien de Chimie Moléculaire, 4 Place Jussieu, Paris, France. E-mail: riccardo.mobili@sorbonne-universite.fr

^c Department of Chemistry, Life Science and Environmental Sustainability University of Parma, Parco Area delle Scienze 17/A, 43124, Parma, Italy

† Electronic supplementary information (ESI) available: Experimental details and methods, syntheses and characterisation, cyclic voltammetry, high-resolution mass spectra (HRMS); ¹H- and ¹³C-NMR, ¹H–¹³C-HSQC, NOESY, DOSY spectra; crystallization data; computational analysis; details on VT-NMR and VT-UV-vis studies. CCDC 2332708. For ESI and crystallographic data in CIF or other electronic format see DOI: <https://doi.org/10.1039/d4cc00812j>



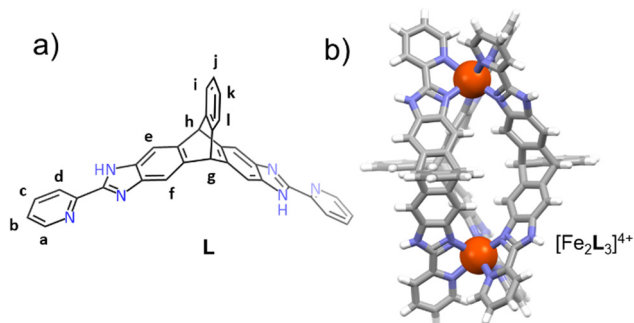


Fig. 1 (a) Sketched structure of the ligand **L** as the “anti” tautomer; (b) structure of the diiron complex $[\text{Fe}_2\text{L}_3]^{4+}$ as obtained from XRD analysis on single crystals (counterions and solvent molecules are omitted for clarity).

ethanol. The dinuclear $\text{Fe}(\text{II})$ and $\text{Zn}(\text{II})$ compounds were obtained as red and yellowish powders, respectively. Both compounds showed good solubility and stability in methanol, ethanol and acetonitrile. Stability is demonstrated by the presence of single species in the NMR spectra of the diiron(II) and dizinc(II) complexes, and the absence of peaks attributed to the free **L** (Fig. S4–S6, S8–S14 and S21, ESI†). On the other hand, decomposition of the diiron assembly in DMSO-d_6 was witnessed by the complex pattern in the ^1H -NMR spectrum (Fig. S20, ESI†).^{11,21a} The HRMS characterization pointed out a 3 : 2 ligand : metal stoichiometry for both the $\text{Fe}(\text{II})$ and $\text{Zn}(\text{II})$ containing species.

Single crystals of the dinuclear $\text{Fe}(\text{II})$ complex were obtained by slow diffusion of diethyl ether into an ethanol solution, and were analyzed through X-ray diffraction at 150 K. The complex crystallizes in the monoclinic space group $P2_1/m$ and the asymmetric unit comprises the moiety $[\text{FeL}_{1.5}](\text{CF}_3\text{SO}_3)_2$ plus water and diethyl ether molecules, some of which highly disordered. As shown in Fig. 1b and in Fig. S19 (ESI†), the diiron complex presents an achiral *meso* structure, in which the three ligands are oriented side-by-side with respect to the two heterochiral (Δ, Λ) metal centres.¹⁴ Each $\text{Fe}(\text{II})$ is coordinated to the sp^2 -hybridized nitrogen atoms within the pyridylimidazole units originating from three distinct ligand strands, effectively locking the imidazole N–H bonds towards the outside of the structure.

The diiron(II) complex, triflate anions and solvent molecules are engaged in several H-bonding interactions,^{15b} specifically involving the benzimidazole NH groups and the O atoms of either CF_3SO_3^- or water (Table S2, ESI†). The two $\text{Fe}(\text{II})$ centres (Fe1, Fe2 in Table 1) are crystallographically equivalent. They exhibit a distorted octahedral geometry, with the six Fe–N bonds having different lengths (a in Table 1). The average

Fe–N bond length, 2.192 Å, is consistent with a high spin (HS) nature for both $\text{Fe}(\text{II})$ centres.^{15a,b} The $\text{Fe}(\text{II}) \cdots \text{Fe}(\text{II})$ distance of 11.119 Å suggests that the metal centres are independent. This was confirmed by cyclic voltammetry (CV) studies on the diiron(II) complex in CH_3CN solution (Fig. S18, ESI†). In particular, a single reversible $\text{Fe}(\text{II})/\text{Fe}(\text{III})$ redox process was observed at $E_{1/2} = +0.48$ V ($\Delta E = 66$ mV) vs. ferrocene/ferrocenium.^{13b}

The structure of the diiron(II) assembly was investigated computationally in the gas phase (refer to Table 1 and Table S3 (ESI†), and Fig. 2).²⁴ The computational analysis† revealed that the only viable configuration for the 2 : 3 $\text{Fe}(\text{II})$: **L** complex corresponded to the *meso* structure. The most stable structure calculated for the mesocate (see the second row in Table 1) exhibits a diamagnetic nature ($S = 0$). The $\text{Fe}(\text{II})$ ions are equivalent ($\text{Fe1}=\text{Fe2}$). The three distances between each $\text{Fe}(\text{II})$ ion and the benzimidazole N atoms ($\text{Fe}-\text{N}_{\text{imz}}$) are equal to each other, as are the distances between each $\text{Fe}(\text{II})$ and pyridines ($\text{Fe}-\text{N}_{\text{py}}$). The calculated average Fe–N distance (2.03 Å) corresponds to a low-spin configuration for both centres (LS–LS).^{12c,15,24} Additionally, two subsequent excited states were identified (relative energy differences are reported in Table 1). Analysis of the Fe–N distances and spin multiplicity indicates that the corresponding structures can be attributed to (i) a complex with $S = 2$, where the two $\text{Fe}(\text{II})$ ions are non-equivalent (HS–LS, as suggested by the corresponding Fe–N distances),^{15,24} (ii) a species with four unpaired electrons per metal centre ($S = 4$), and where the $\text{Fe}(\text{II})$ ions are equivalent (HS–HS). These three states exhibit closely similar structures (see figure in Table S3, ESI†), their similar energies suggest that an easy interconversion between these states can occur even at low temperatures.

An insight into the structure of the diiron(II) complex in solution was obtained by NMR investigations. As anticipated, the ^1H -NMR spectrum of the diiron complex exhibited only one set of signals (in CD_3OD , $T = 298$ K), confirming the presence of a unique and symmetric species in solution (see Fig. S4, ESI†). Strongly down-field/up-field shifted and broadened peaks were also observed, indicating the presence of a HS $\text{Fe}(\text{II})$ complex. The paramagnetic centre had the greatest impact on the protons of the pyridine units and the substituted Tp blades. On the other hand, the bridgehead protons and those associated with the non-substituted blade were less affected, with their signals falling in the diamagnetic region (Fig. S5 and S6, ESI†). Protons Hg and Hh gave two distinct singlets, confirming that the ligands are in the *syn* tautomer even in solution. This result is also consistent with the mesocate structure as determined by both SCXRD and DFT

Table 1 Selected bond lengths in the crystal (a), and in optimised structures (gas phase) (b). N_{imz} , N_{py} : atoms belonging to benzimidazoles and pyridines, respectively. Fe1, Fe2: $\text{Fe}(\text{II})$ centres; ΔE : relative energy differences for the optimised structures

	Fe– N_{imz} (Å)	Fe– N_{py} (Å)	ΔE (kcal mol ^{−1})
Fe1=Fe2 ^(a)	2.139(2), 2.146(2), 2.151(2)	2.229(2), 2.240(2), 2.249(2)	
Fe1=Fe2 ^(b)	2.02	2.04	0
Fe1 ^(b)	2.02	2.04	12.5
Fe2 ^(b)	2.01, 2.14, 2.15	2.02, 2.18, 2.29	
Fe1=Fe2 ^(b)	2.00, 2.13, 2.16	2.02, 2.18, 2.29	25



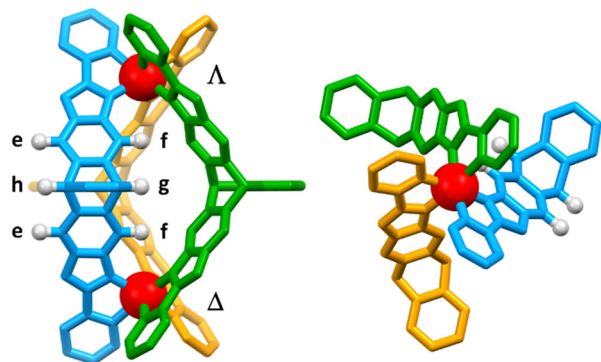


Fig. 2 Lateral and top views of the optimized structure of the HS-HS ($S = 4$) diiron complex $[\text{Fe}_2\text{L}_3]^{4+}$.

calculations. Additional information about the chemical environment of the protons were provided by the ^1H -NMR analysis on the diamagnetic $\text{Zn}(\text{II})$ analogue (Fig. S8 and S9, ESI †). Similarly to the $\text{Fe}(\text{II})$ mesocate, a single set of ^1H -NMR peaks was found. Furthermore, two singlets were detected for the bridgehead protons Hg and Hh. The substantial separation ($\Delta\delta \approx 1.93$ ppm) between these two protons can be rationalized based on the mesocate structure, in which the corresponding Hg protons are oriented towards the shielding cone of a neighbouring ligand. The couples of protons (Hg,Hh) and (He,Hf) actually experience a different chemical environment, and become symmetrically inequivalent (see Fig. 1b and 2). Through NMR findings, it has been confidently established that dimerization is not occurring for these complexes under the experimental conditions used. In particular, a diffusion-ordered spectroscopy (DOSY) experiment conducted on the dizinc complex in CD_3CN revealed a hydrodynamic radius value consistent with the expected size for the M_2L_3 species (Fig. S14, ESI †).

The paramagnetic character of the diiron mesocate was investigated in solution through the variable temperature (VT) ^1H -NMR Evans method.^{17,18,20} In particular, the magnetic susceptibility was determined on a CD_3OD solution of the diiron complex (2.3 mM) in the temperature range 193–293 K

(Fig. 3) using chloroform as standard. $\chi_m T$ values, calculated for a single $\text{Fe}(\text{II})$ centre (see the ESI †), went from $2.67 \text{ cm}^3 \text{ mol}^{-1} \text{ K}$ (293 K) to $0.64 \text{ cm}^3 \text{ mol}^{-1} \text{ K}$ (193 K), (Fig. S22, ESI †), indicating a transition from HS to LS state. The experimental data were then fitted to the regular solution model ‡ as a one-step SCO event.¹⁸ The obtained transition enthalpy and entropy (ΔH and ΔS , $12.9 \text{ kJ K mol}^{-1}$ and 52.9 J mol^{-1} , respectively) are consistent with the values reported for similar diiron-based SCO systems. In the investigated temperature range, the HS fraction of the diiron complex goes from 0.75 to 0.16 (at 293 K and 193 K, respectively), thus indicating a quasi-total spin conversion with a $T_{1/2}$ of 243 K. The ΔH and ΔS values provide a negative Gibbs free energy at 298 K (-2.9 kJ mol^{-1}), thus confirming the stabilization of the HS state for the complex at room temperature. The obtained results were confirmed by variable temperature UV-vis spectroscopy investigations (Fig. 4). ‡ The VT experiment was performed between 193 K and 313 K on a 75 μM solution of the complex in methanol. The molar absorptivity (ϵ) of the charge-transfer band at 528 nm increases on decreasing temperature, varying between $2.4 \times 10^3 \text{ M}^{-1} \text{ cm}^{-1}$ (313 K) to $9.4 \times 10^3 \text{ M}^{-1} \text{ cm}^{-1}$ (193 K). § The change in the intensity of this band is consistent with the increasing low-spin fraction at low temperatures. The molar absorptivity values per $\text{Fe}(\text{II})$ centre were then plotted to the HS fraction obtained by the Evans method (see Fig. S26, ESI †). The linear fitting revealed a correlation between ϵ values (at 528 nm) and the HS fraction, enabling the determination of the molar absorptivity of the LS species ($\epsilon_0 = 1.1 \times 10^4 \text{ M}^{-1} \text{ cm}^{-1}$ per complex). The ϵ_0 was ultimately utilized to fit the experimental molar absorptivity values with the regular solution model, treating it as a one-step SCO event, and to calculate the thermodynamic parameters ΔH and ΔS (12.6 kJ mol^{-1} and $51.5 \text{ J K}^{-1} \text{ mol}^{-1}$, respectively). The $T_{1/2}$ was found to be in very good agreement with that obtained by the Evans method, yielding a value of 245 K.^{19–22}

In this work, we report the first example of Tp-based triple-stranded mesocates, with $\text{Fe}(\text{II})$ and $\text{Zn}(\text{II})$ as octahedral metal centres. The metal-induced self-assembly stabilizes the *syn* form of the partially adaptive ligand, leading to the formation of M_2L_3 complexes in which the side-by-side disposition of the ligands is likely imposed by the rigid molecular skeleton and by

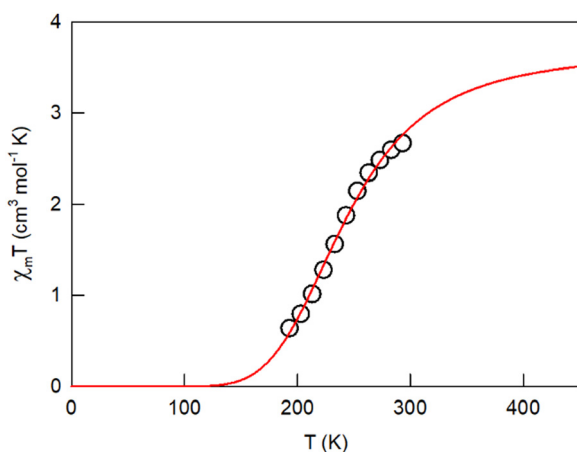


Fig. 3 Plot of $\chi_m T$ vs. T for a 2.3 mM solution (4.6 mM in $\text{Fe}(\text{II})$) of $[\text{Fe}_2\text{L}_3](\text{CF}_3\text{SO}_3)_4$ in CD_3OD from Evans method NMR studies (400 MHz). Black dots: experimental data; red curve: fitted model from eqn (S2) (ESI †).

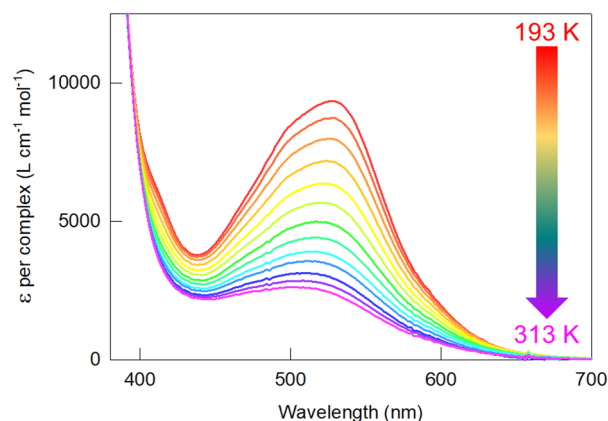


Fig. 4 Variable temperature UV-vis study of a 0.075 mM solution of $[\text{Fe}_2\text{L}_3](\text{CF}_3\text{SO}_3)_4$ in methanol (path-length = 1 cm).



the steric effect of triptycenes. These factors prevent the three ligand strands from wrapping around the two metal centres, thereby precluding the formation of a helicate structure. The self-assembly is therefore diastereoselective, promoting the formation of the mesocate species only. In addition, studies on the diiron(II) mesocate in solution showed that the complex is paramagnetic at room temperature, and undergoes a thermal-induced one-step SCO with $T_{1/2}$ at 243 K (Evans method). This result, confirmed by variable-temperature UV-visible studies in the same medium, contrasts with observations in the crystalline state, where Fe–N distances were consistent with a HS–HS configuration at 150 K. However, this discrepancy can be explained by intermolecular hydrogen bonding interactions in the crystal packing, which freeze the Fe(II) ions in their high-spin state,^{15e} and by the relatively small energy difference between LS/HS states, as determined by computational studies.

To the best of our knowledge, the system described in this manuscript represents the inaugural instance of a triptycene-based supramolecular assembly incorporating Fe(II) and exhibiting spin-crossover in solution. These results not only can contribute to the fundamental understanding of supramolecular chemistry (aromatic ligands with a rigid framework typically favor the formation of helicate complexes),^{12,13} but also hold promise for the utilization of triptycene derivatives in various technological applications,^{1,2,8} ranging from molecular switches and sensors to advanced materials for electronics, optoelectronics, and beyond.^{15–23}

We acknowledge the Ministero dell'Università e della Ricerca (MUR) and the University of Pavia through the program “Dipartimenti di Eccellenza 2023–2027”. We acknowledge the CINECA award under the ISCRA initiative, for the availability of high-performance computing resources and support. S. Tarantino (UniPV), M. Zema (UniBA), B. Mannucci and T. Recca of the Centro Grandi Strumenti (UniPV) are thanked for technical support. Chiesi Farmaceutici SpA is acknowledged for the support with the D8 Venture X-ray equipment. RM: conceptualisation, synthesis, data analysis; GP: synthesis; EM: VT studies; DD, SV: DFT calculations; CM: SCXRD; DP: supervision; VA: writing, supervision.

Conflicts of interest

There are no conflicts to declare.

Notes and references

- (a) J. H. Chong and M. J. MacLachlan, *Chem. Soc. Rev.*, 2009, **38**, 3301–3315; (b) T. M. Swager, *Acc. Chem. Res.*, 2008, **41**, 1181–1189; (c) C. Chen and Y. Han, *Acc. Chem. Res.*, 2018, **51**, 2093–2106; (d) M. Woźny, A. Mames and T. Ratajczyk, *Molecules*, 2022, **27**, 250; (e) L. Ueberricked and M. Mastalerz, *Chem. Rec.*, 2021, **21**, 558–573.
- (a) G. Preda, A. Nitti and D. Pasini, *ChemistryOpen*, 2020, **9**, 719–727; (b) G. Preda, R. Mobili, D. Ravelli, V. Amendola and D. Pasini, *J. Org. Chem.*, 2024, **89**(8), 5690–5698.
- (a) M. J. Gu, Y. F. Wang, Y. Han and C. F. Chen, *Org. Biomol. Chem.*, 2021, **19**, 10047–10067; (b) S. La Cognata, A. Miljkovic, R. Mobili, G. Bergamaschi and V. Amendola, *ChemPlusChem*, 2020, **85**, 1145–1155; (c) K. Omoto, S. Tashiro and M. Shionoya, *Chem. Sci.*, 2019, **10**, 7172–7176.
- Y. Li, R. Cao and S. J. Lippard, *Org. Lett.*, 2011, **13**, 5052–5055.
- S. Hasegawa, S. L. Meichner, J. J. Holstein, A. Baksi, M. Kasanmascheff and G. H. Clever, *J. Am. Chem. Soc.*, 2021, **143**(26), 9718–9723.
- (a) J. Sanmartin-Matalobos, M. Fondo, A. M. Garcia-Deibe, M. Amoa, P. Bermejo, M. R. L. Dominguez, A. J. Mota, J. L. Perez-Lustres, S. Bhowmick and N. Das, *RSC Adv.*, 2016, **6**, 21228–21234; (b) X. S. Du, Y. Han and C. F. Chen, *Chem. Commun.*, 2022, **58**, 1326–1329.
- (a) K. Oki, W. Zheng, E. Yashima and T. Ikai, *Chem. Commun.*, 2023, **59**, 8989–8992; (b) T. Ikai, T. Yoshida, K. Shinohara, T. Taniguchi, Y. Wada and T. M. Swager, *J. Am. Chem. Soc.*, 2019, **141**(11), 4696–4703.
- (a) Y.-F. Wang, M. Li, J.-M. Teng, H.-Y. Zhou and C.-F. Chen, *Adv. Funct. Mater.*, 2021, **31**, 2106418; (b) R. Ammenhäuser, J. M. Lupton and U. Scherf, *Adv. Opt. Mater.*, 2024, **12**, 2301857; (c) G. Preda, A. Aricò, C. Botta, D. Ravelli, D. Merli, S. Mattiello, L. Beverina and D. Pasini, *Org. Lett.*, 2023, **25**, 6490–6494.
- A. Vuillamy, S. Zebret, C. Besnard, V. Placide, S. Petoud and J. Hamacek, *Inorg. Chem.*, 2017, **56**, 2742–2749.
- S. Chakraborty, S. Mondal, S. Bhowmick, J. Ma, H. Tan, S. Neogi and N. Das, *Dalton Trans.*, 2014, **43**, 13270–13277.
- H. Zhu, T. K. Ronson, K. Wu and J. R. Nitschke, *J. Am. Chem. Soc.*, 2024, **146**, 2370–2378.
- (a) J.-M. Lehn, *Supramolecular Chemistry—Concepts and Perspectives*, VCH, Weinheim, 1995; (b) C. Piguet, G. Bernardinelli and G. Hopfgartner, *Chem. Rev.*, 1997, **97**, 2005–2062; (c) L. J. Charbonnière, A. F. Williams, C. Piguet, G. Bernardinelli and E. Rivara-Minten, *Chem. – Eur. J.*, 1998, **4**, 485–493.
- (a) V. Amendola, M. Boiocchi, V. Brega, L. Fabbriizzi and L. Mosca, *Inorg. Chem.*, 2010, **49**, 997–1007; (b) P. Pallavicini, V. Amendola, Y. Diaz Fernandez, M. Ghisalberti, L. Linati, C. Mangano, A. Manotti Lanfredi and C. Massera, *Dalton Trans.*, 2003, 575–580; (c) V. Amendola, M. Boiocchi, V. Brega, L. Fabbriizzi and L. Mosca, *Inorg. Chem.*, 2010, **49**, 997–1007.
- (a) M. Albrecht, *Chem. Eur. J.*, 2000, **6**(19), 3485–3489; (b) B. H. Wilson, H. S. Scott, O. T. Qazvini, S. G. Telfer, C. Mathonière, R. Clérac and P. E. Kruger, *Chem. Commun.*, 2018, **54**, 13391–13394; (c) D. J. Cooke, J. M. Cross, R. V. Fennessy, L. P. Harding, C. R. Rice and C. Slater, *Chem. Commun.*, 2013, **49**, 7785–7787; (d) J. Xu, T. N. Parac and K. N. Raymond, *Angew. Chem., Int. Ed.*, 1999, **38**(19), 2878–2882.
- (a) R. W. Hogue, S. Singh and S. Brooker, *Chem. Soc. Rev.*, 2018, **47**, 7303–7338; (b) F. Tuna, M. R. Lees, G. J. Clarkson and M. J. Hannon, *Chem. – Eur. J.*, 2004, **10**, 5737–5750; (c) K. S. Kumar, Y. Bayeh, T. Gebretsadiq, F. Elemo, M. Gebrezgabher, M. Thomas and M. Ruben, *Dalton Trans.*, 2019, **48**, 15321–15337; (d) L. Wu, M. Tang, L. Jiang, Y. Chen, L. Bian, J. Liu, S. Wang, Y. Liang and Z. Liu, *Nat. Synth.*, 2023, **2**, 17–25; (e) J. Wang, Y. Li, R.-J. Wei, Z. Tang, Z.-S. Yao and J. Tao, *Inorg. Chem.*, 2023, **62**(4), 1354–1361.
- M. A. Halcrow, *Spin-Crossover Materials: Properties and Applications*, John Wiley & Sons, Ltd, Chichester, 1st edn, 2013.
- Q. M. Phung, A. Domingo and K. Pierloot, *Chem. – Eur. J.*, 2018, **24**, 5183–5190.
- D. Jyoti Mondal, A. Gupta and S. Konar, *Chem. – Eur. J.*, 2023, e202300060.
- S. Singh and S. Brooker, *Chem. Sci.*, 2021, **12**, 10919–10929.
- L. L. K. Taylor, I. J. Vitorica-Yrezabal, I. Borilović, F. Tuna and I. A. Riddell, *Chem. Commun.*, 2021, **57**, 11252–11255.
- (a) M. Darawsheh, L. A. Barrios, O. Roubeau, S. J. Teat and G. Aromí, *Chem. – Eur. J.*, 2016, **22**, 8635–8645; (b) D. Y. Aleshin, R. Diego, L. A. Barrios, Y. V. Nelyubina, G. Aromí and V. V. Novikov, *Angew. Chem., Int. Ed.*, 2022, **61**, e202110310.
- S. Z. Zhao, H. W. Zhou, C. Y. Qin, H. Z. Zhang, Y. H. Li, M. Yamashita and S. Wang, *Chem. – Eur. J.*, 2023, **29**, e202300554.
- S. G. Telfer, B. Bocquet and A. F. Williams, *Inorg. Chem.*, 2001, **40**, 4818–4820.
- R. Kulmaczewski, I. T. Armstrong, P. Catchpole, E. S. J. Ratcliffe, H. B. Vasili, S. L. Warriner, O. Cespedes and M. A. Halcrow, *Chem. – Eur. J.*, 2023, **29**, e20220257.

